Journal of Achievements in Materials and Manufacturing Engineering
VOLUME 43
ISSUE 1
November
2010

Computer modelling of ductile iron solidification using FDM and CA methods

W. Kapturkiewicz*, A.A. Burbelko, E. Fraś, M. Górny, D. Gurgul
Faculty of Foundry Engineering, AGH University of Sciences and Technology,
ul. Reymonta 23, 30-059 Kraków, Poland
* Corresponding author: E-mail address: kaptur@agh.edu.pl

Received 25.09.2010; published in revised form 01.11.2010

Analysis and modelling

ABSTRACT

Purpose: The purpose of the work was the presentation of tool for modelling of solidification process, for prediction of some structure parameters in DI by the given chemical composition of alloy and for given boundary condition of casting.
Design/methodology/approach: Two mathematical models and methods developed by authors have been presented: micromodelling with using of finite difference method (FDM) and mesomodelling with using of cellular automaton method (CA).
Findings: The FDM was used for solving the DI so¬lidification model, including heat conductivity equation with source function, boundary condition for casting, equations for austenite and eutectic grains nucleation depended on the changing undercooling, the Weibull's formula for graphite nodule count, Kolmogorov's equation for calculation of volume fraction of phases (eutectics and austenite). A set of equations, after transformation to a differ¬ence form, were solved by the finite difference method, using an iteration procedure. The correctness of the mathematical model has been experimen¬tally verified in the range of most significant factors, which include temperature field, the value of maximum undercooling, and the graphite nodule count interrelated with the casting cross-section. Literature offers practi¬cally no data on so confronted process model and simulation program. The CA model was used for the simulation of the grains' shapes in connection with FD for temperature field and solute redistribution in the grain scale.
Practical implications: FDM modeling gives the possibility of statistical description of microstructure but the geometrical shape of grains is assumed a priori. In CA modeling the grain shape is not assumed, but this is the result of modeling. The use of FDM gives results quantitatively comparable to the process in real casting, particularly according to temperature fields and number of graphite spheroids.
Originality/value: The CA method gives on the present stage credible qualitative results but this method is more perspective for good reproducing of the real process of solidification.
Keywords: Computational materials science; CA; FDM; Modelling; Ductile iron, Solidification

Reference to this paper should be given in the following way:
W. Kapturkiewicz, A.A. Burbelko, E. Fraś, M. Górny, D. Gurgul, Computer modelling of ductile iron solidification using FDM and CA methods, Journal of Achievements in Materials and Manufacturing Engineering 43/1 (2010) 310-323.

1. Introduction

The structure of alloys formed during solidification affects the properties of casting. This is the reason why in modern metallurgy and the related technological processes the possibility of modelling the structure formation process is so important, especially if different aspects of this complex phenomenon can be taken into consideration. The eutectic microstructure is a result of a simultaneous growth of two (or more than two) solid phases from the melt. This structure is a base of numerous technical alloys. The physical and mechanical properties of such materials depend not only on the properties and volume fraction of each phase but also on the morphology of grains.

The microstructure peculiarity of the DI is a spheroidal shape of the grains of one phase – graphite. Another phase growing directly from the melt during the solidification is the austenite. The graphite and austenite grains are nucleated in the liquid phase. At first these grains grow directly from the melt. Next the austenite shell arises all around of the graphite nodules. This envelope isolates the graphite grains from the liquid phase. From this moment the graphite grains grow due to the carbon diffusion from liquid solution to the nodules surface through the solid solution layer. The austenite grains still solidify directly from the melt but on the border "graphite nodule – austenite envelope" this phase vanishes and releases the volume for spheroid growth. The Cellular Automaton (CA) is one of the known methods of the simulation of microstructure formation during the solidification used in the multiscale modelling [1, 2].

The first mathematical model of the dendritic solidification of the metals and alloys based on the method of CAFD (Cellular Automata – Finite Differences) was presented by Umantsev at al. [3]. The next publication that was written by the same authors disclosed the obtained by modelling effect of initial undercooling on the morphology of thermal dendrite and structure evolution of its secondary arms in micro-scale [4].

In the CA modelling the outer grain shape and inner properties (e.g. secondary dendrite arm space, solute distribution in the solids etc.) are the results of the simulation and do not superimposed beforehand. In the modelling the following physical phenomenon are taken into account: releasing of the latent heat of phase transformations in the phase interface and heat flow, the solutes redistributions between the different phases and diffusion mass transport, the equilibrium temperature changes near the curved grain boundaries (Gibbs-Thomson effect.) It is possible to take into consideration the non-equilibrium character of the phase transformations. The models development for a one-phase microstructure evolution is a subject of the numerous research [5-14]. The question of the eutectic solidification in the superimposed temperature condition was solved in [15-18].

The purpose of the present work is a two-dimension model development for simulation of the DI structure formation during the solidification in the condition of non steady-state temperature. Model takes into account the continuous nucleation, separate growth of graphite nodules and austenite dendrites at the first solidification stage, and the following cooperative growth of graphite-austenite eutectic in the binary Fe-C system.

The mechanical, physical and utilization properties of this cast iron depend on the number of the graphite grains and on the individual matrix constituents. The prediction of local properties of castings is an old dream of foundrymen and casting designers which nowadays is becoming every day more true due to the development of our computational abilities. To predict the mechanical properties of nodular graphite iron it is necessary to simulate the refinement and volume fraction of the individual structural constituents present in this cast iron.

Most of the computer modelling programs described in literature are devoted to eutectic transformation [19-24] under the preassumed stationary conditions of carbon diffusion in austenite. In [23] a physical model of solidification of the nodular graphite cast iron which quantitatively accounts for the formation of non-eutectic austenite during cooling and solidification of hypereutectic as well as hypoeutectic cast iron has been presented. In investigation [24], process modelling techniques have been applied to describe the multiple phase changes occurring during solidification and subsequent cooling of near-eutectic nodular graphite cast iron, based on the internal state variable approach. The diffusion model of graphitization in nodular cast iron casting has been presented in [25].

According to [26], below the eutectic temperature, austenite dendrites and graphite spheroids can nucleate independently in the liquid. This mechanism has been confirmed by both [27, 28] for hypo-eutectic and eutectic, as well as hyper-eutectic SGI.

Concluding from that, it has been introduced by [29] formulae uninodular models assume a basic unit of solidification formed by a graphite nodule and austenite shell covering the nodule, and multinodular ones assume that each unit of solidification is formed by a grain of dendritic austenite containing several graphite spheres. Celentano et al. [29] has presented model, in which velocity of nucleation depends on current liquid fraction. There is no justification of this thesis, and the consistency between the model and experiment has been obtained through properly selected values of the coefficients b and c, and by mere comparison of the cooling curves, without analysis of the nodule count obtained by computations and in experiment.

The aim of this study, using FDM – Finite Difference Method, at the second part of this work was to develop a model of SGI solidification, using knowledge available so far, confronted with an experiment in respect of both the cooling curves as well as the grain distribution and graphite nodule count in real casting.

2. FD method [30]

2.1. Model of process

The model combines a macro model (heat transfer in casting) with micro model (nucleation and growth of grains). Heat transfer in casting depends on the cooling conditions created by foundry mould.

According to the analysis of reference literature presented above, it has been assumed that, irrespective of the fact that molten metal may have the chemical composition corresponding to a eutectic one (carbon equivalent CE≈1.0), it is possible that austenite dendrites and graphite spheroids will nucleate independently in the liquid. The mechanism of the diffusion growth of nodular graphite (allowed for in, among others, [31]) has been disregarded, assuming that the leading factor in the process of the

grain growth is the kinetic undercooling at an austenite-liquid phase boundary, including the growth of both eutectic grains and austenite dendrites (for which an approximate spherical growth with amendment in Kolmogorov equation has been adopted). It has also been assumed that the eutectic nodule count is equivalent to graphite nodule count.

The macro temperature field in casting-mold system is:

$$\frac{\partial T}{\partial \tau} = a\nabla^2 T + \frac{q_s}{c_v}, \tag{1}$$

Where: T, τ – temperature and time, a – thermal diffusivity (for metal or for mold), q_s – heat generation rate of phase transformations, c_v – volumetric specific heat.

In order to calculate the true volume fraction of solid, one must include the effect of grain impingement. The true volume fraction of solid f_S can be described by Kolmogorov equation [31]:

$$f_S = 1 - e^{-\Omega}, \tag{2}$$

where Ω - so-called "extended" volume of all solid grains.

According to Kolmogorov [31]:

$$\Omega = -\frac{4\pi}{3} s \int_0^t \alpha(t') \left(\int_{t'}^t u(\tau) d\tau \right)^3 dt' \tag{3}$$

where t' - nucleation time, $\alpha(t')$ - rate of the grain nucleation, $u(\tau)$ – linear velocity of the growth ($\int_{t'}^{t} u(\tau) d\tau$ – grain radius), s – shape coefficient (e.g. s=1 for globular grains and s=0.3 for dendrite grains).

It is well known that liquid cast iron contains undissolved particles of various sizes. Hence, upon alloy undercooling beyond a critical value, these particles exceed the minimum sizes needed for stable growth. Hence, growing nuclei are continually developed until the time when the metal attains its maximum level of undercooling. Afterward, with the progress of recalescence, no new nuclei form because all the particles larger than the critical size (which corresponds to maximum undercooling) were already exhausted. Activation of smaller particle substrates as active nuclei will require undercooling, which will have to exceed the maximum value. To compute the density of the formed austenite nuclei the following relationship has been adapted [32]:

$$N_\gamma = \psi_\gamma \ \Delta T_\gamma^2 \tag{4}$$

where $\Psi\gamma$ – nucleation coefficient of austenite grains, ΔT_γ – undercooling with the reference to equilibrium austenite temperature.

For number of graphite nodule count the Weibull formula (after Fraś [33]) has been used:

$$N_e = N_s \exp\left(-b/\Delta T_e\right) \tag{5}$$

where: N_s – overall nucleation site density in the melt, b – nucleation coefficient, ΔT_e – undercooling with the reference to equilibrium eutectic temperature.

The austenite linear growth velocity the classic law [34] is used:

$$u_\gamma = \mu_\gamma \Delta T_\gamma^{2.5} \tag{6}$$

where μ_γ – austenite growth coefficient.

Rate of growth for eutectic grains [35]:

$$u_e = \mu_e \cdot \Delta T_e^2 \tag{7}$$

where:μ_e – eutectic growth coefficient.

The equilibrium temperatures T_γ for solidifying austenite and T_e for eutectics can be represented by linear functions of carbon, silicon and phosphorus concentration in liquid cast iron [36, 37]:

$$T_\gamma = 1636 - 113\left(C_L + 0.25\,Si_L + 0.5\,P_L\right) \tag{8}$$

$$T_e = 1154 + 5.25\,Si_L - 14.88\,P_L \tag{9}$$

where: C_L, Si_L, P_L – weight percent of C, Si and P in liquid.

According to Kobayashi [35] the solute concentration in the solidifying phases is strongly influenced by the magnitude of the diffusion coefficients. Hence, for solute of relatively high diffusivity (e.g. carbon in austenite), the solute concentration in the liquid phase can be approximated by the mass balance. Alternatively, the Scheil equation can be used in dealing with low diffusivity solutes, such as in the case of silicon or phosphorus in austenite.

A set of the above equations, after transformation to a differential form, was solved by the finite difference method, applying an iteration procedure (secant method). The simulation program operating in Delphi environment was prepared in 1D and 3D systems.

The verification of the developed model was confronted with the results of an experiment which in more detail was described in [37].

The parameters adopted in modelling are given below and in Table 1 and 2. The first five parameters in Table 2 concern the nucleation and growth, the next ones – thermal conductivity, specific heat and density for casting and mould material. The results of experiments (and cooling curves from experiments) from Tab. 3 were taken for compare with modelling.

2.2. Parameters of experiment and for modelling

Table 1.
Chemical composition of cast iron, wt% [37]

Melt No.	C	Si	P	CE	Std. deviation of CE
1	3.62	2.68	0.020	1.0496	0.002
2	3.73	2.57	0.013	1.0705	0.006
3	3.62	2.65	0.014	1.0463	0.004
Mean value	3.66	2.63	0.016	1.055	

Table 2.
Parameters for modelling

Property	Value	Units
Ψ_γ	$5x10^6$	$cm^{-3}\ K^{-2}$
μ_γ	$5x10^{-5}$	$cm\ s^{-1}\ K^{-2}$
N_s	$5x10^7$	cm^{-3}
b	50	K
μ_e	$1x10^{-7}$	$cm\ s^{-1}\ K^{-2}$
λ_c	0.37	$W\ cm^{-1}\ K^{-1}$
c_c	0.753	$J\ cm^{-3}\ K^{-1}$
ρ_c	7.3	$g\ cm^{-3}$
L_γ	1952.4	$J\ cm^{-3}$
L_e	2028.8	$J\ cm^{-3}$
λ_m	0.0103	$W\ cm^{-1}\ K^{-1}$
c_m	1.09	$J\ cm^{-3}\ K^{-1}$
ρ_m	1.73	$g\ cm^{-3}$

Volumetric graphite count was calculated using Wiencek [38] expression:

$$N_v = \sqrt{\frac{N_A^3}{V_{gr}}} \tag{10}$$

where V_{gr} is volumetric fraction of graphite, with $V_{gr} \approx 0.1$.

Table 3.
Experimental results [38]

Melt No.	Plate thickness, cm	Max. undercooling, K	Graphite nodule count	
			Planar N_A, $cm^{-2}x10^2$	Volumetric N_v, $cm^{-3}x10^6$
1	0.6	45	270	14.0
3	0.6	49	327	18.6
	1.6	26	130	4.7
4	0.6	43	313	17.5
	1.0	33	324	10.6

2.3. Discussion of the results by FD method

The development of computer program, basing on the assumed mathematical model of the solidification process of casting made from nodular graphite iron, had as a main objective checking the viability and reproducibility of this model, and investigating some of its specific features. Selected elements of the model (temperature field, number of grains) were verified by experiments. The successful results of this verification have confirmed the assumptions made previously that the developed model faithfully reflects the reality. Assuming now the correct functioning of mathematical model and of the respective simulation program enabling practical operation of this model, numerous process-related results were obtained. Although, so far, not all of them have been checked in practical application, they can still give important information on the mechanism of the examined process. The aim of the computations was, besides analysis of the solidification process examined in selected places of casting, determination of differences that occur in this process on casting cross-section.

The simulation computations were carried out on plates of three different cross-sections. The thermophysical parameters were taken from the data given in literature. The plate geometry and the starting test conditions were adapted to those applied previously in the experiment. Castings of the shape of rectangular prism had the thickness of 6, 10 and 16 mm; the remaining dimensions were kept constant for all the thickness values and amounted to 100 x 100 mm. Castings were made in ceramic moulds. Detailed description of the experimental conditions was given in [37].

From the casting geometry as stated above (the length of the casting sides exceeds many times its thickness in the ratios of 16.6, 10 and 6.25, respectively), it follows that the three-dimensional problem (3-D) can be converted into a one-dimensional problem (1-D), much easier and quicker in computations. To check this well-known hypothesis, appropriate computations were made to compare the results obtained on 1-D and 3-D models. For a 16 mm plate, the difference in the solidification time amounted to about 40%, for the thickness of 6 mm – to about 2%. For all the thickness values, the run of the cooling curves was practically identical until the end of recalescence (the relevant drawings were not inserted here because of the lack of space). Hence a conclusion follows that to determine the structure-related parameters (e.g. the grain count in individual phases), a quickly-operating 1-D variant of the program can be used for all of the above mentioned thickness values. On the other hand, when the solidification time or the curve run at the end of the solidification process has to be computed for plates of the side length-to-thickness ratio below 15, the use of 3-D program is recommended.

Figures 1-2 show the run of the cooling curves plotted for an interior part of the 6, 10 and 16 mm plates. The curves drawn in solid line represent the simulation results, while dots show the experimental values according to [37]. Figure 1 shows the results obtained for three melts (the chemical composition is given in Table 1), while other two drawings (Figs. 2 and 3) show the results of an experiment carried out on one melt. A good compatibility has been obtained between the results computed for the initial stage of the process. Differences at the end of casting solidification are most probably due to the fact that the model does not allow for variations in thermophysical properties of molding material, due to the thermal effect of liquid metal.

For more detailed analysis, some of the results were presented in an enlarged scale. Figure 4 shows the results obtained on a 6 mm thick cast plate in the temperature range of 1100-1200ºC. The dotted line marks the run of the equilibrium temperature curve of eutectic transformation Te and of the equilibrium liquidus temperature curve plotted for a Fe-C system (including the effect of Si and P) and the middle part of casting. The differences in the values of the equilibrium temperature and real temperature, i.e. the undercooling, will make the subject of further analysis.

The temperature curves from both simulation (solid line) and experiment (dotted line) shows „sagging" marked with letter A. Their presence is due to the effect of the nucleating and growing grains (dendrites) of austenite.

Some attention deserves the fact that studies in both variants, i.e. simulation and experiment, were carried out on the Fe-C-Si-P alloy of practically eutectic composition (the point of eutectic saturation C_E= 1.05) which, considering an equilibrium course of the solidification process, allows us to expect total absence of the austenite in structure.

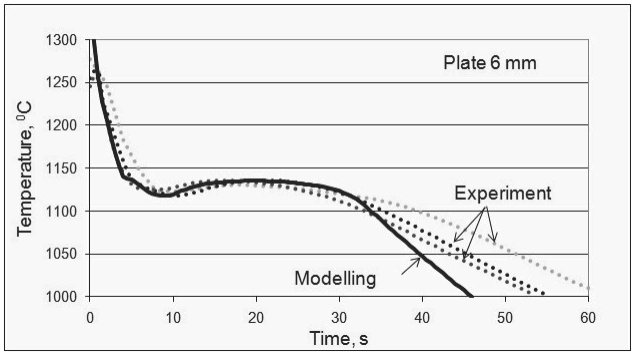

Fig. 1. Cooling curves plotted for an interior part of the 6 mm plate.

Yet, modelling carried out for a non-equilibrium system has revealed an important share of austenite (disclosed in further drawings).

Another proof is the result of modelling excluding the possibility of austenite nucleation – Figure 5, where the plotted cooling curve is basically different from both the experimental curve (dots) and simulation curve (solid line). The said drawing, displaying the results obtained on a 10 mm thick cast plate, also shows the characteristic point A, which reflects the thermal effect caused by the growing dendrites of austenite. Figure 6 shows differences in the run of the cooling curves plotted for the cast plate of 10 mm thickness, and differences in the run of the equilibrium temperature curves plotted for eutectic transformation.

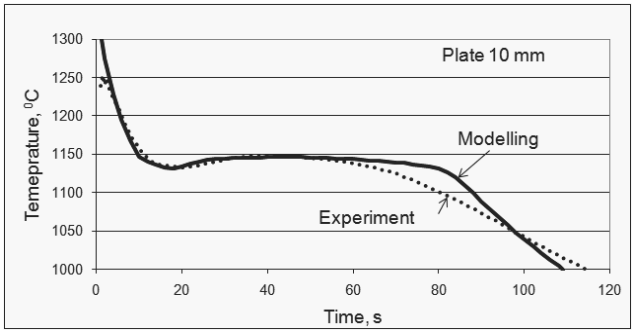

Fig. 2. Cooling curves for an interior part of the 10 mm plate

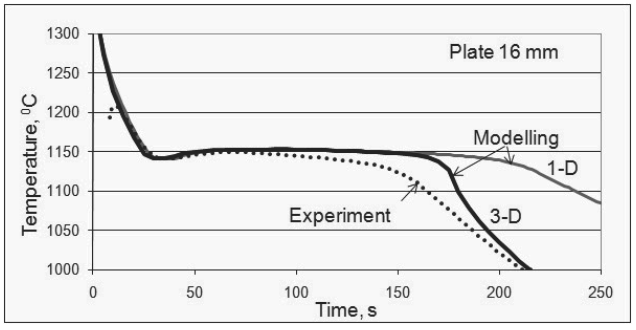

Fig. 3. Cooling curves plotted for an interior part of the 10 mm plate

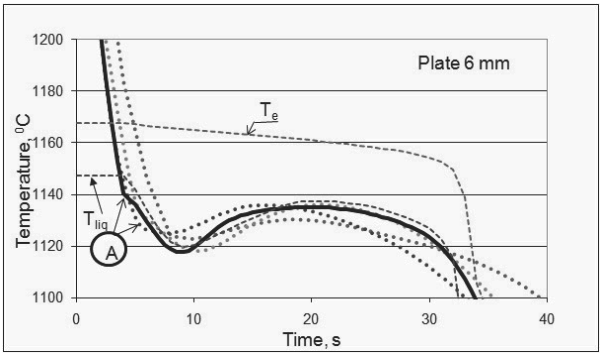

Fig. 4. Results obtained on a 6 mm thick cast plate in the temperature range of 1100-1200^{0}C

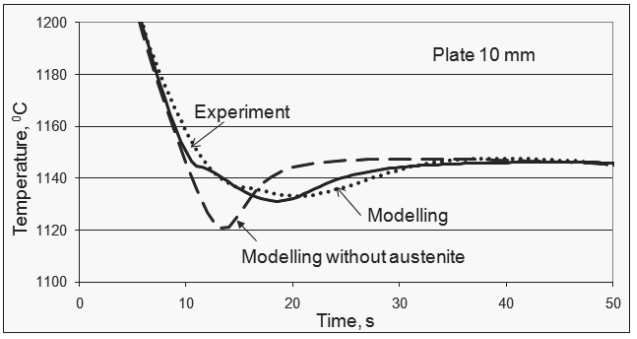

Fig. 5. Modelling with excluding and including the possibility of austenite nucleation

Hence, a conclusion follows that when only one value of the equilibrium temperature is adopted in computations of the undercooling, the result can be burdened with a significant error.

Quite characteristic is also the stronger thermal effect of austenite (point A) in the middle part of casting, as compared to the surface (Fig. 6).

From Figures 7 and 8 it follows that, under given conditions, the nucleation of austenite and eutectic takes place almost at the same time. Similar as in the remaining drawings, point A on the curve of eutectic nucleation (Fig. 8) indicates an indirect effect of the austenite growth. The thermal effect of the austenite growth arrests the temperature drop, which is directly responsible for the reduced rate of eutectic grains nucleation.

A comparison of Figures 7 and 8 shows that rate nucleation of austenite grains is a little higher than the nucleation rate of eutectic. From Figures 9 and 10 it follows that the growth rate of austenite grains is also higher of that observed in eutectic.

Figure 11 shows the kinetics of the grain radius growth in austenite and eutectic. The differences in the kinetics of this growth are visible on the casting cross-section. With the kinetics of growth varying on the casting cross-section, after the solidification, different final values of the austenite grain radius (equivalent to dendrite volumes) were obtained, while final size of the eutectic grains remained practically the same on the entire casting cross-section.

The final number of eutectic grains depends on the value of maximum undercooling which, in turn, depends on process parameters. For the same melt, the same pouring temperature, casting

configuration and mould material, it depends on the casting thickness only, as shown in Figures 12 and 13. With increasing casting thickness, the value of the maximum undercooling is decreasing, analogically to the number of eutectic grains (in nodular graphite cast iron associated rather with the count of graphite nodules). The values obtained by modelling (solid line) have been compared with the values measured in experiments. Besides comparison of the cooling curves, this is the most significant criterion to evaluate the correctness of a mathematical model of the process and of the developed simulation program.

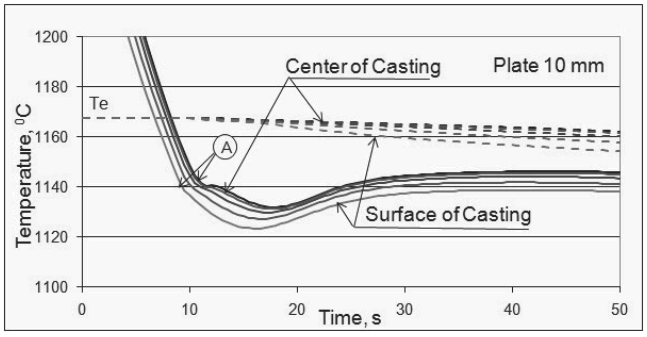

Fig. 6. Cooling curves and equilibrium eutectic temperature in section of casting (modelling)

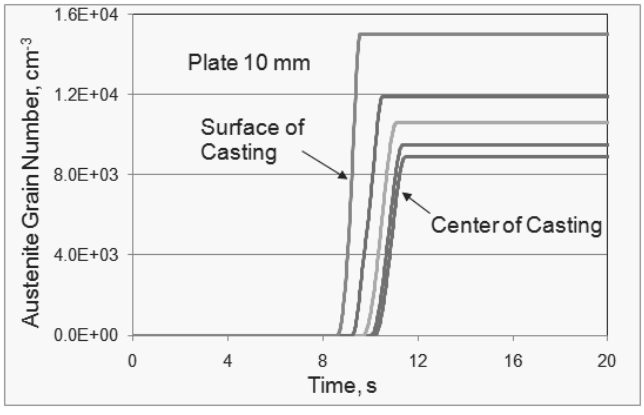

Fig. 7. Kinetics of austenite grains nucleation (modelling)

Figure 14 shows small differences in the final volume of austenite and eutectic on the casting cross-section, where the distinguishing feature is a relatively high volume content of austenite (about 23 – 25%) in alloy of the eutectic saturation ratio equal to 1.05, which de facto means a eutectic alloy. As mentioned previously, it is the consequence of allowing for non-equilibrium conditions of the solidification process.

One of the most important factors that influence cast iron solidification is the segregation of alloying constituents, i.e. of silicon and phosphorus. In a schematic process representation, the Scheil model was adopted (full mixing of the constituent in liquid phase, lack of diffusion in solid phase), disregarding the flow (mixing) of constituents between different elements of the computational grid, which in practice means different places in casting. The segregation of constituents allowing for non-equilibrium process conditions is best reflected in the distribution silicon and phosphorus on the cross-section of austenite grains - Figures 15-16 – and in eutectic – Figures 17-18. Strong segregation of silicon has been observed to take place in the grains of both austenite and eutectic (at grain boundaries its content approaches zero) and phosphorus, the content of which has been rapidly increasing along the grain boundaries of both austenite and eutectic.

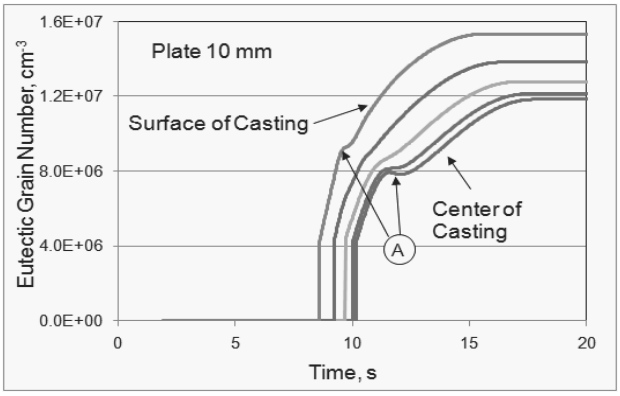

Fig. 8. Kinetics of eutectic grains nucleation (modelling)

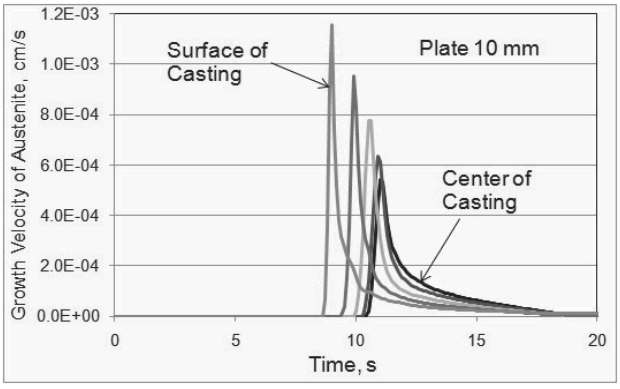

Fig. 9. Austenite growth velocity (modelling)

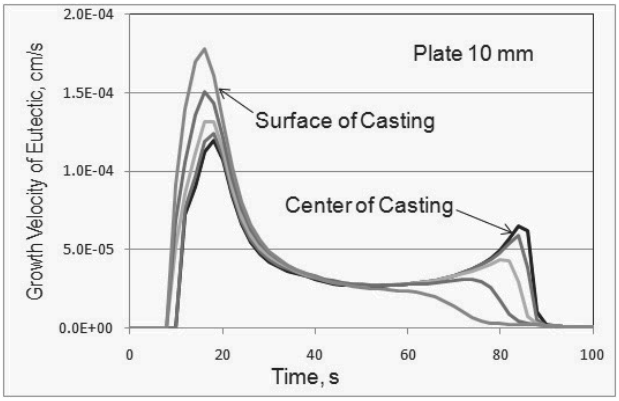

Fig. 10. Eutectic growth velocity (modelling)

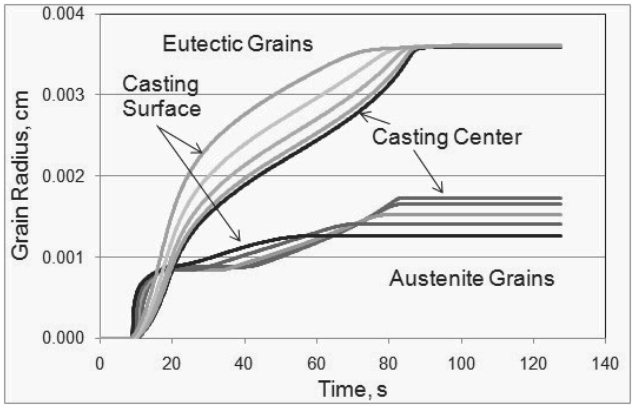

Fig. 11. Kinetics of austenite and eutectic growth (modelling)

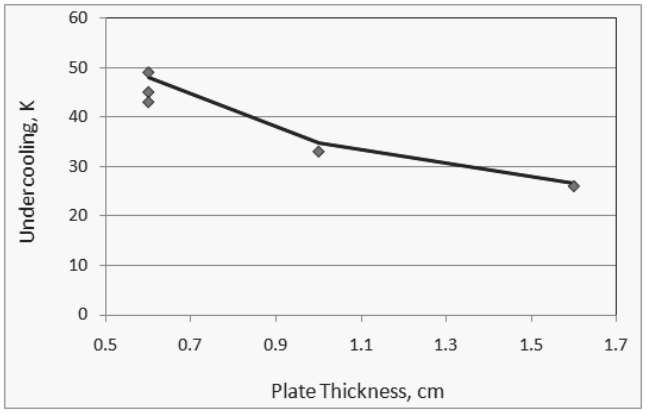

Fig. 12. Maximum undercooling versus casting plate thickness. Line – modelling; points – experiment

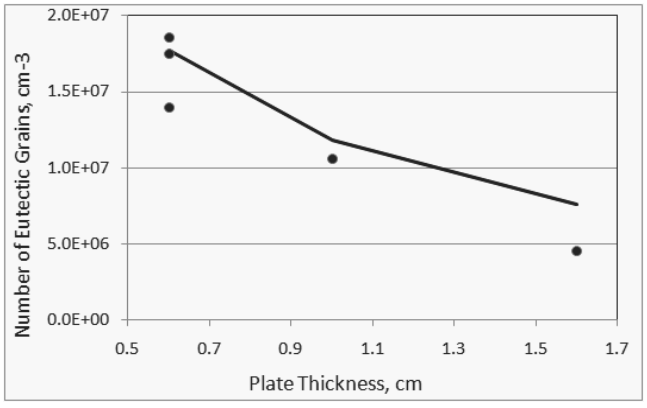

Fig. 13. Number of eutectic grains (nodule count) versus casting plate thickness. Line – modelling; points – experiment

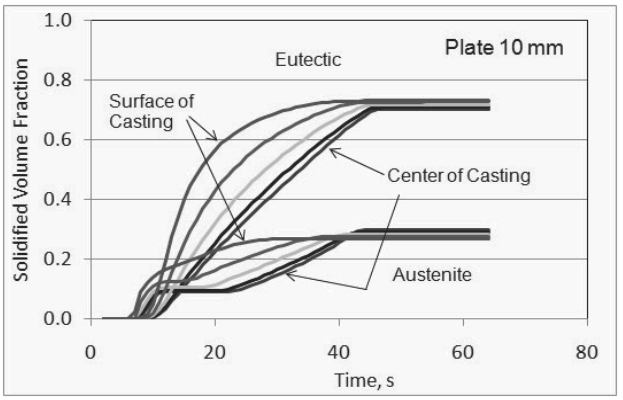

Fig. 14. Kinetics of austenite and eutectic volume fraction (modelling)

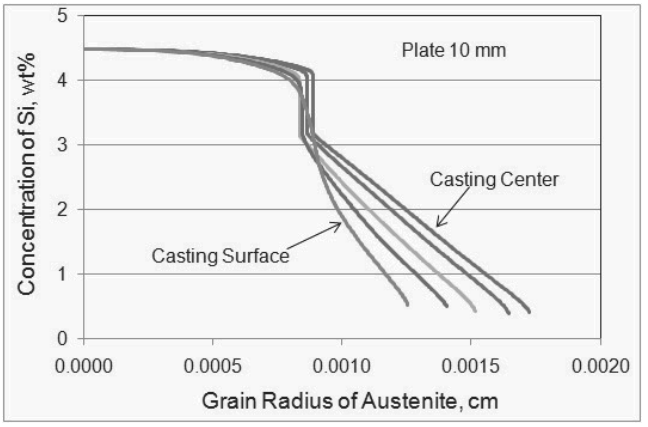

Fig. 15. Distribution of silicon on the cross-section of austenite grains

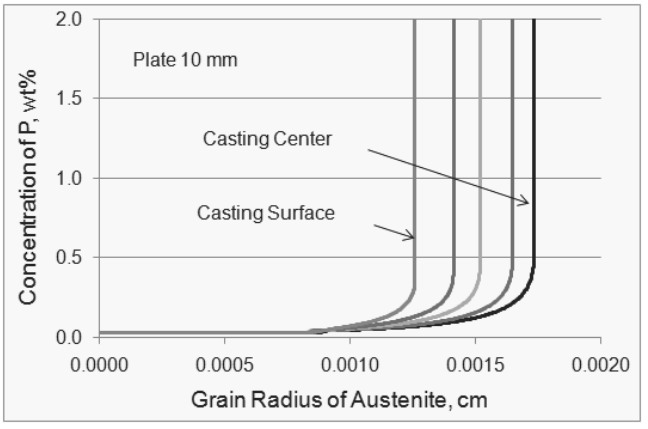

Fig. 16. Distribution of phosphorus on the cross-section of austenite grains

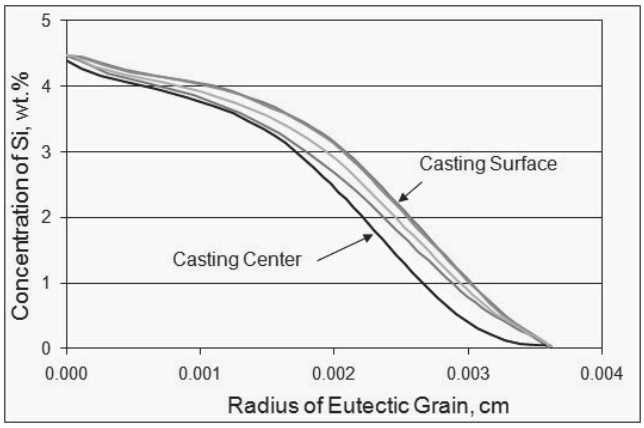

Fig. 17. Distribution of silicon on the cross-section of eutectic grains

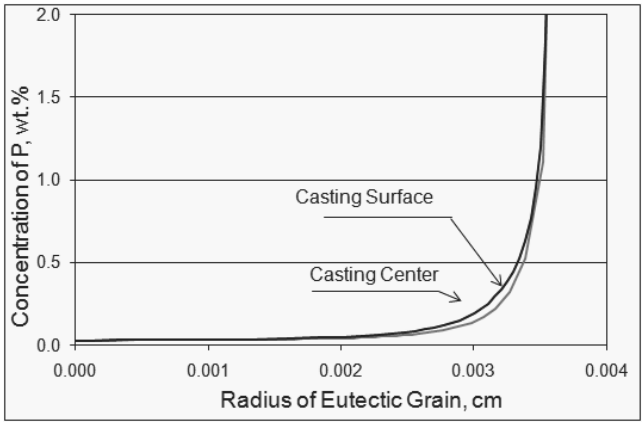

Fig. 18. Distribution of phosphorus on the cross-section of eutectic grains

Considering the adopted model of segregation, one can expect that the numerical values of the segregation of constituents (Figs. 15-18) will be less differentiated in reality, but qualitatively the results are relevant and fully justified.

In the developed model of nodular graphite iron casting solidification, the correctness of the mathematical model has been experimentally verified in the range of the most significant factors, which include temperature field, the value of maximum undercooling, and the graphite nodule count interrelated with the casting cross-section. Literature offers practically no data on so confronted process model and simulation program.

Undoubtedly, an experimental verification of other results obtained by simulation is recommended, especially as regards the content of austenite and eutectic on the casting cross-section, and the segregation of constituents on the grain section under given process conditions. It also seems advisable to allow in mathematical model for deviations from the Scheil model, i.e. taking into account the diffusion in liquid phase with possible partial mixing, and for diffusion in the solid phase.

3. CA method

3.1. Model description and solution method

Cellular Automaton is an idealization of a real system in which space, time, and the states of a cell are discrete [39]. Presented model uses set of 6 cell states for microstructure modelling: 3 mono-phase states "liquid", "austenite", and "graphite", and 3 two-phase states.

In the beginning all cells of CA lattice are in the "liquid" state. The analyzed domain is cooled with a constant cooling rate. When the temperature of liquid drops down below the liquidus the nucleation and growth of grains can be possible.

The kinetic undercooling of the mother liquid phase is a measure of the thermodynamic driving force of new growth of grains. Total undercooling on the solidification front, hence the difference between equilibrium solidification temperature T_{Eq} (determined from the phase equilibrium diagram for carbon concentration obtained during simulation on the transformation front) and real temperature T_r is equal to the sum of capillary undercooling ΔT_κ and kinetic undercooling ΔT_μ (see Fig. 19):

$$T_{Eq} - T_r = \Delta T_\kappa + \Delta T_\mu \tag{11}$$

where $\Delta T_\kappa = \Gamma\kappa$, Γ is the Gibbs-Thomson coefficient, and κ is a front curvature.

The scheme of liquidus lines positions with accounting of capillary effect for convex grains is shown in Fig. 19. by dashed lines.

Basing on [40], it has been assumed in the computations that the interface migration rate is a linear function of local kinetic undercooling ΔT_μ:

$$u = \mu \Delta T_\mu \tag{12}$$

where μ is the kinetic growth coefficient.

The increment of new phase volume fraction in the interface cells Δf over the one time step $\Delta\tau$ in the square CA cells of size a was calculated according to the equation proposed in [41]:

$$\Delta f = \frac{u\,\Delta\tau}{a\left(|\cos\theta| + |\sin\theta|\right)} \tag{13}$$

where θ is the angle between the X axis and normal direction of grain interface.

If the phase volume fraction in the interface cell increase up to 1, this cell exchange they state from interface to appropriate one-phase. In addition this cell captures all adjacent ones: theirs states exchange to appropriative interface. It is a well known fact, that heat and mass diffusion processes in a liquid in front of the solidification interface results in the growth of the disturbance with a low curvature. On the other part, perturbations with a high curvature are dampening down by surface energy of the interphase boundary [42].

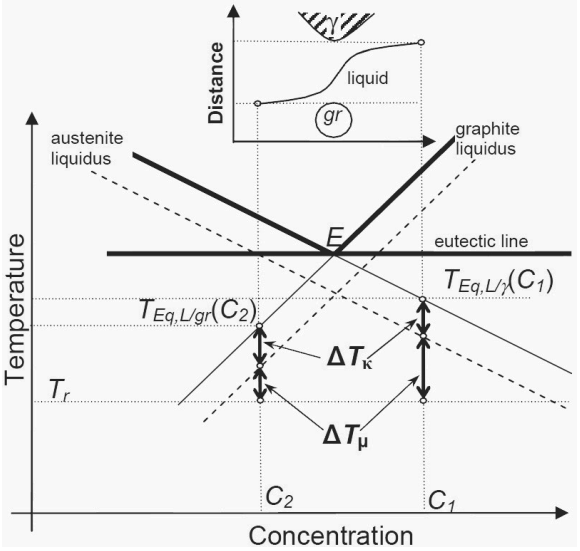

Fig. 19. Scheme of the iron-carbon binary phase diagram.

The results of it are known morphological changes of the growing grains boundary shapes with the changes of growth velocity: plain, cellular, dendritic, seaweed, and fractal. The computer modelling of the heat and mass diffusion processes together with the growing grain shape simulation by cellular automata method make possible to predict the structure evolution of metallic alloy during the solidification.

For the heat flow in the analyzed domain the numerical solution of nonlinear Fourier equation was used:

$$c\frac{\partial T}{\partial \tau} = \nabla(\lambda \nabla T) + q_T + q_{cool} \tag{14}$$

where: T is the temperature, τ is the time, λ is the thermal conductivity, c is the volumetric specific heat. Two source terms are used: q_{cool} is the intensity of the external cooling, and q_T is a latent heat generation rate as a consequence of phase transformation.

The solute diffusion in the domains of every phase was calculated like the temperature distribution, by the numerical solution of diffusion equation with a source term in the solidification front:

$$\frac{\partial C}{\partial \tau} = \nabla \cdot (D \nabla C) + q_C \tag{15}$$

where D is the solute diffusion coefficient, C is the solute concentration in this phase, q_C is a source term as a consequence of the carbon redistribution between the phases.

Carbon concentration in the graphite is always equal to 1. For the "austenite-liquid" interface:

$$C_\gamma = kC_L \tag{16}$$

where k is the solute partition coefficient, C_γ, C_L are the carbon concentration in the austenite and liquid.

The Eqs. (14) and (15) were solved by Finite Differences Method. The implicit scheme was used. The solution of Eq. (15) was obtained on the dense lattice with the same spatial step with the lattice of CA (overlapped mesh.) Maximum time step of implicit scheme for Eq. (14) solution for the temperature field for this lattice is about 10^4 times shorter. That is why the another lattice (the sparse one) was used with a multiple spatial step and the same time discretization. The temperature of the interface cells was calculated by linear interpolation from the nodes of sparse lattice.

Both source functions are equal to zero outside the interface cells. In the interface cells the value of the heat and mass sources for the finite-difference scheme are:

$$q_T = L_{\alpha\to\beta}\frac{\Delta f_\beta}{\Delta \tau} \tag{17}$$

$$q_C = (C_\alpha - C_\beta)\frac{\Delta f_\beta}{\Delta \tau} \tag{18}$$

where $L_{\alpha\to\beta}$ is the volumetric latent heat of α→β transformation, C_α and C_β are the carbon concentration in the vanishing and growing phases, and Δf_β is the growth of the new phase volume fraction during the time step Δτ.

The source function (17) calculated for the elements of the dense mesh was integrated over the area of the elements of sparse one.

The normal direction of grain boundary in the interface cells was determined by the approach of **F**-vector [43]. The angle θ between the growth direction (normal to the grain boundary) and positive X-axis direction was calculated as follow:

$$\theta = \arctan\left(\sum_{i,j} y_{i,j} f_{i,j} \Big/ \sum_{i,j} x_{i,j} f_{i,j}\right) \tag{19}$$

where: $f_{i,j}$ is the volume fraction of the phase in the cell (i,j) $x_{i,j}$, $y_{i,j}$ are the relative coordinates of adjacent cells. The summation in (19) over the 20 neighbour cells gives the best results of normal direction estimation [44].

The liquidus lines in the binary Fe-C thermodynamic diagram were approximated by linear function using the data from [45].

3.2. Nucleation modelling

The number of active substrates in the domain V of the melt with an undercooling ΔT below the liquidus may be calculated on the basis of the cumulative distribution function $F(\Delta T)$:

$$N = N_{\max} F(\Delta T) V \tag{20}$$

where: N_{max} is the maximum specific number of substrates for nucleation.

When one substrate position doesn't have any influence on another substrate's positions, the random variable calculated as the number of substrates in any random domain V will have the Poisson statistical distribution with the mean value $\nu = N_{max}V$. For this statistical distribution the probability density function is

$$P_r(k) = e^{-\nu}\nu^k/k! \tag{21}$$

where: e is the Euler-Mascheroni constant, and k is the estimated number of substrates.

The method of nucleation modelling for a CA lattice is known [46]. According to this method the undercooling values randomly generated with a statistical distribution curve are attributed to randomly chosen cells. If a cell is chosen several times (i.e., if it contains more than one nucleation site), only the smaller nucleation undercooling is used.

If the CA cell is too high/large in size, the calculated grain density will be underestimated. A modified version of this algorithm was used in this paper.

First of all, the advisable relation between a cell's volume (or surface for 2D) υ and the substrate density must be estimated. The probability of the lack of a nucleus in the cell ($k = 0$) according to Poisson's statistic is equal to:

$$P_r(k=0) = e^{-\nu} \tag{22}$$

The probability of one substrate ($k = 1$) in the cell is represented by the following equation:

$$P_r(k=1) = \nu e^{-\nu} \tag{23}$$

The probability of more than one substrates in one cell may be calculated as:

$$P_r(k>1) = 1 - \nu e^{-\nu}(1+\nu) \tag{24}$$

For the small ν $e^{-\nu} \approx 1-\nu$, we will hereby use the following equation:

$$P_r(k>1) = \nu^2 \tag{25}$$

The mean number of cells in a CA lattice with M_{CA} cells where more than one substrate is located is equal to $M_{CA}\cdot\nu^2$. Because $\nu = N_{max}\cdot\upsilon$, the next criterion may be proposed for an estimation of the correct nucleation model using:

$$M_{CA}(N_{max}\upsilon)^2 < K \tag{26}$$

When the above inequality is true, the mean number of cells in a CA lattice where more than one substrate is present will be less than K.

The next way of substrate placement and the undercooling of nucleation selection is proposed based on the mean number of active substrates in one cell:

$$\nu = N_{max}F(\Delta T)\upsilon \tag{27}$$

For each of the cells in the CA a random number p should be generated with an equiprobability distribution in the (0..1] range. The condition of the substrate present in the cell is the following inequality:

$$p < N_{max}F(\Delta T)\upsilon \tag{28}$$

The nucleation undercooling in this case should be estimated on the basis of the inverse function of the above-mentioned cumulative distribution curve (fractile):

$$\Delta T = F^{-1}(p) \tag{29}$$

The solid grain will begin to grow when the undercooling exceeds the above level. The substrates are present (and nucleation is possible) only in cells with a positive ΔT value.

The Weibull statistical distribution was used in this paper for nucleation modeling. The specific number of active substrates is given by [33]

$$n = N_{\max}\exp(-b/\Delta T) \tag{30}$$

where b is a nucleation coefficient.

The undercooling of nucleation can be calculated as

$$\Delta T = -b\Big/\ln\left(\frac{p}{\upsilon N_{\max}}\right) \tag{31}$$

The values for N_{max} and b used in the present work for the modelling of graphite and austenite grains nucleation are listed in Table 4.

Table 4.
Nucleation parameters

	Austenite	Graphite
b, K	300	5
N_{max}, m^{-2}	$1.5\cdot10^7$	$1.0\cdot10^9$

3.3. Results of CA computations

Computations were carried out on a grid of 640×640 cells. The length of the side of a cell was 1 μm. A uniform starting distribution of the carbon concentration in the binary Fe-C liquid was assumed, equal to 0.0425 part of the mass fraction. Basing on [45], as an equilibrium coefficient of carbon distribution between the liquid phase and austenite, $k_C = 0.4941$ was adopted. Other thermophysical parameters that were used in the modelling are shown in the Table 5.

For the thermal and carbon concentration fields the periodic boundary conditions were used described in [39]. The intensity of the external cooling rate was equal 10 K/s (if $q_T = 0$).

The results of modelling are presented in the Fig.20. All graphite grains in this figure are black.

a)

b)

c)

d)

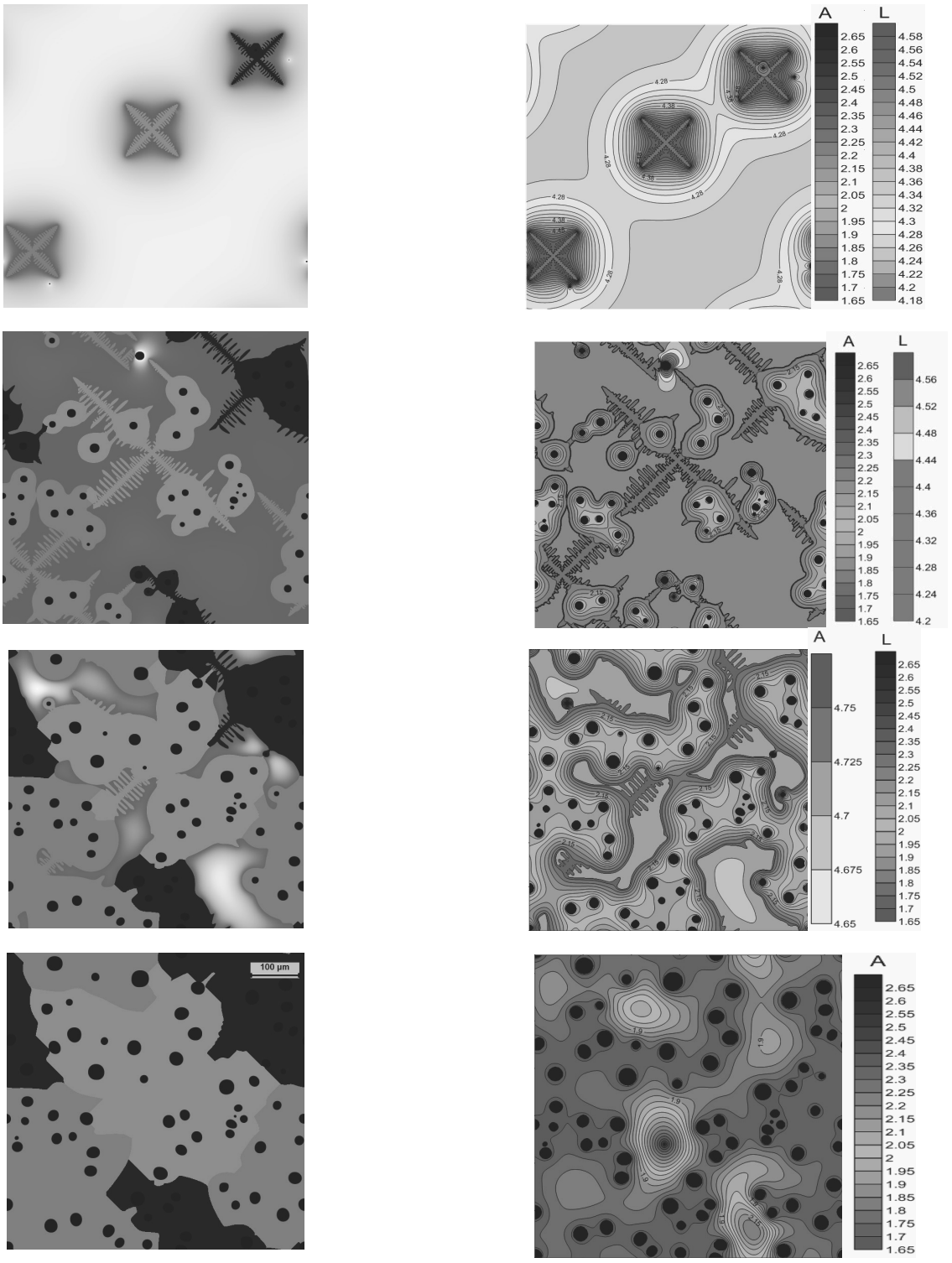

Fig. 20. The stages of DI microstructure formation (modelling); time, s: a) 5.1; b) 17.7; c) 33.0; d) 47.8 and isolines of the carbon concentration in the austenite (scale A) and liquid (scale L) – right side (cont.)

The austenite grains have different colour level (constant for each grain). Right side of the pictures shows the concentration map.

As graphite nodules, as austenite dendrites nucleate from the liquid. During crystallization from the liquid phase ahead of the austenite growth front, a liquid zone rich in carbon is formed. The solubility of carbon in the growing solid phase is lower than in the disappearing liquid phase. A reverse situation occurs in the liquid ahead of the front of graphite growth. In places where the distance between the growing phases is not large enough, a soft collision occurs, and due to this effect the concentration fields start acting on the growing grains, destroying the symmetry of their growth. If this collision occurs in the case of two identical grains (austenite-austenite or graphite-graphite), their growth will be arrested in the direction of the collision.

Table 5.
Thermophysical parameters used in the modelling.

		Liquid	Austenite	Graphite
Heat conductivity, λ	W/(m·K)	30	20	40
Specific heat, c	J/(m^3·K)	$5.6 \cdot 10^6$	$5.84 \cdot 10^6$	$1.78 \cdot 10^6$
Density, ρ	kg/m^3	7000	7300	2230
Carbon diffusivity, D	m^2/s	$1.25 \cdot 10^{-9}$	$5.0 \cdot 10^{-10}$	0
		Austenite-liquid	Graphite-liquid	Austenite-graphite
Latent heat	J/m^3	$19.7 \cdot 10^8$	$16.2 \cdot 10^5$	$8.8 \cdot 10^5$
Gibbs-Thomson coefficient	m·K	$1.9 \cdot 10^{-7}$	$7.0 \cdot 10^{-6}$	$9.5 \cdot 10^{-6}$
Growth coefficient	m/(s·K)	10^{-4}	10^{-7}	10^{-7}

The soft collision of the grains of different phases (providing a phase rich in carbon, e.g. graphite, appears near the growing austenite grain) increases the carbon diffusion flow in direction between the phases. In this case, carbon concentration decreases ahead of the austenite grain growth front, and increases ahead of the graphite growth front. The concentration gradient of the dissolved constituent increases, resulting in accelerated diffusion mass transport. At the same time, with the above mentioned changes of concentration profile in the liquid phase, the undercooling increases at both solidification fronts.

The thermodynamic driving force of the crystallisation of both phases increases, resulting in accelerated migration of the grain boundaries towards each other. The scheme of the carbon distribution in the liquid between the austenite and graphite grains (with a non-equilibrium border concentration on both interfaces) is shown in the top part of the Fig. 19.

As it follow from the Fig. 21, each austenite grain can coverage several graphite nodules. This results are in the good correlation with the experimental investigation of solidification structure of DI [47,48]. Fig. 21 shows changes of the dendrite surface shape with a time step equal to 2 s. Final shape of the border between the two dendrites is visible as a border of different colours.

Cooling curve obtained in the CA modelling is shown in Fig. 22. The shape of this cooling curve with recalescence is typical for DI. It is similar to the further results obtained by FDM method.

4. Conclusions

In the developed model of nodular graphite iron casting solidification, the correctness of the mathematical model has been experimentally verified in the range of the most significant factors, which include temperature field, the value of maximum undercooling, and the graphite nodule count interrelated with the casting cross-section. Literature offers practically no data on so confronted process model and simulation program.

It has been showed, that in eutectic cast iron (CE =1) the nucleation and growth of austenite grains are of great importance. The cooling curves of modelling with excluding and including the possibility of austenite nucleation are quite different and the experimental curve is close to the case with austenite.

Undoubtedly, an experimental verification of other results obtained by simulation is recommended, especially as regards the content of austenite and eutectic on the casting cross-section, and the segregation of constituents on the grain section under given process conditions. It also seems advisable to allow in mathematical model for deviations from the Scheil model, i.e. taking into account the diffusion in liquid phase with possible partial mixing, and for diffusion in the solid phase.

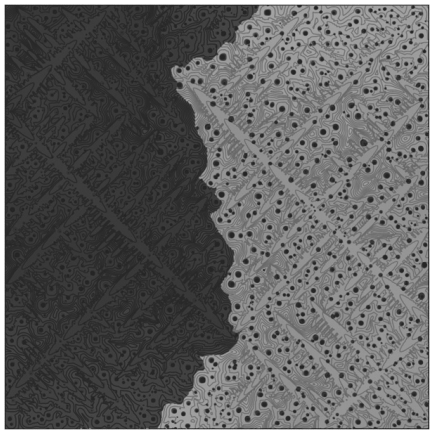

Fig. 21. Sample of the solidification front position in the different time of solidification (modelling)

It has been proved in CA modelling that the rate of growth of the austenite dendrite branches can increase during simulation if a grain of graphite is placed nearby. After enclosing of the graphite nodules by the austenite, further growth of graphite is possible because the carbon diffuses from liquid solution to the nodules surface through the solid solution layer. It was shown, that each austenite grain can coverage several graphite nodules. These results are in the good correlation with the experimental investigation.

FDM modeling gives the possibility of statistical description of microstructure (number and size of grains, volume fraction of structure component, diversity of chemical composition in cross of grains but the geometrical shape of grains (both single or multiphase) is assumed a priori. In CA modeling the grain shape is not assumed, but is the result of modeling.

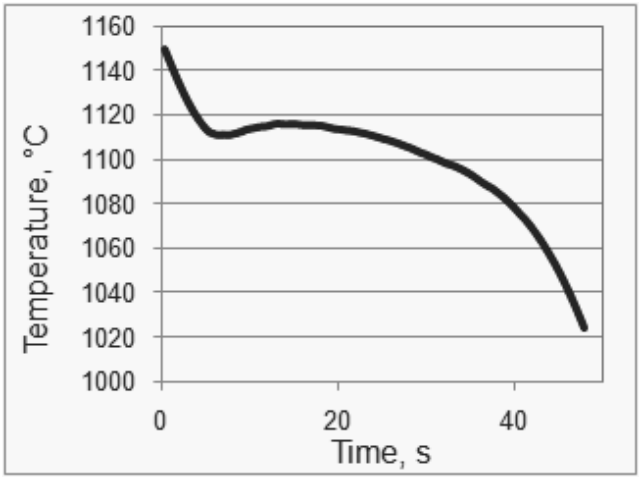

Fig. 22. Cooling curve obtained in the CA modelling

Using of FDM gives the results quantitatively comparable with the process in real casting, particularly according to temperature fields and number of graphite spheroids. The CA method gives on the present stage the credible qualitative results but this method is more perspective for good reproducing of the real process of solidification.

Acknowledgements

The work was supported by Polish MNiSW Project No. N507 422536.

References

[1] H. Rafii-Tabar, A. Chirazi, Multi-scale computational modelling of solidification phenomena, Physics Reports - Review Section of Physics Letters 365 (2002) 145-249.
[2] P.D. Lee, A. Chirazi, R.C. Atwood, W. Wang, Multiscale modelling of solidification microstructures, including microsegregation and microporosity, in an Al-Si-Cu alloy, Materials Science and Engineering A 365 (2004) 57-65.
[3] A.R. Umantsev, V.V. Vinogradov, V.T. Borisov, Mathematical modeling of the dendrite growth in the undercooled melt, Kristallografia 30 (1985) 455-460 (in Russian).
[4] A.R. Umantsev, V.V. Vinogradov, V.T. Borisov , Modeling of the dendrite structure evolution, Kristallografia 31 (1986) 1002-1008 (in Russian).
[5] M. Rappaz, Ch.A. Gandin, Probabilistic modeling of microstructure formation in solidification processes, Acta Metallurgica et Materialia 41 (1993) 345-360.
[6] S. Pan, M. Zhu, A three-dimensional sharp interface model for the quantitative simulation of solutal dendritic growth, Acta Materialia 58 (2010) 340-352.
[7] S. Mosbah, M. Bellet, Ch.A. Gandin, Simulation of solidification grain structures with a multiple diffusion length scales model, in Modeling of Casting, Welding and Advanced Solidification Processes - XII, TMS, Vancouver, Canada, 2009, 485-493.
[8] G. Guillemot, Ch.A. Gandin, M. Bellet, Interaction between single grain solidification and macro segregation: application of a cellular automaton - finite element model, Journal of Crystal Growth 303 (2007) 58-68.
[9] G. Guillemot, Ch.A. Gandin, M. Bellet, Interaction between single grain solidification and macro segregation: application of a cellular automaton - finite element model, Journal of Crystal Growth 303 (2007) 58-68.
[10] V. Pavlyk, U. Dilthey, Simulation of weld solidification microstructure and its coupling to the macroscopic heat and fluid flow modelling, Modelling and Simulation in Materials Science and Engineering 12 (2004) 33-45.
[11] M.F. Zhu, C.P. Hong, A three dimensional modified cellular automaton model for the prediction of solidification microstructures, ISIJ International 42 (2002) 520-526.
[12] D.J. Jarvis, S.G.R. Brown, J.A. Spittle, Modelling of non-equilibrium solidification in ternary alloys: comparison of 1D, 2D, and 3D cellular automaton-finite difference simulations, Materials Science and Technology 16 (2000) 1420-1424.
[13] A.A. Burbelko, E. Fraś, W. Kapturkiewicz, Modelling of dendritic growth during unidirectional solidification by the method of cellular automata, Materials Science Forum 649 (2010) 217-222.
[14] A.A. Burbelko, E. Fraś, W. Kapturkiewicz, E. Olejnik, Nonequilibrium kinetics of phase boundary movement in cellular automaton modelling, Materials Science Forum 508 (2006) 405-410.
[15] S.G.R. Brown, N.B. Bruce, Three-dimensional cellular automaton models of microstructural evolution during solidification, Journal of Materials Science 30 (1995) 1144-1150.
[16] MF. Zhu, CP. Hong, Modeling of microstructure evolution in regular eutectic growth, Physical Review B 66/155428 (2002) 1-8.
[17] M.F. Zhu, C.P. Hong, Modeling of microstructure evolution in eutectic and peritectic solidification, Modeling of Casting, Welding and Advanced Solidification Processes - X, TMS, Warrendale, Pennsylvania, 2003, 91-98.
[18] M.F. Zhu, C.P. Hong, D.M. Stefanescu, Y.A. Chang: Computational modeling of microstructure evolution in solidification of aluminum alloys, Metallurgical and Materials Transactions 38B (2007) 517-524.
[19] D.M. Stefanescu, A. Catalina, X. Guo, L. Chuzhoy, M.A. Pershing, G.L. Biltgen, Prediction of room temperature mcrostructure and mechanical properties in iron castings, in Modeling of Casting, Welding and Advanced Solidification Process, The Minerals, Metals and Materials Society 1998, 455-462.
[20] S.M. Yoo, A. Ludwig, P.R. Sahm, Numerical simulation of nodular cast iron in permanent moulds, Solidification Processing, Renmor House, Univ. of Sheffield 1997, 494-497.
[21] S. Chang, D. Shangguan, D.M. Stefanescu, Modeling of the liquid/solid and the eutectoid phase transformation in spher-

oidal graphite cast iron, Metallurgical and Materials Transactions 23A (1992) 1333-1346.
[22] T. Skaland, O. Grong, T. Grong, A model for the graphite formation in ductile cast iron, Metallurgical and Materials Transactions 24A (1993) 2347-2353.
[23] G. Lesoult, M. Castro, J. Lacaze, Solidification of spheroidal graphite cast iron, Acta Metallurgica et Materialia 46, (1998) 983 -995, 997-1010.
[24] M.I. Onsoien, O. Grong, O. Gundersen, T. Skaland, A process model for the micro-structure evolution in ductile cast iron: part I, Metallurgical and Materials Transactions 30A (1999) 1053-1068.
[25] E. Fraś, W. Kapturkiewicz, A.A. Burbelko, H.F Lopez, Modeling of graphitization kinetics in nodular cast iron casting, in: Modeling of Casting, Welding and Advanced Solidification Processes IX, Aachen, Shaker 2000, 885-892.
[26] D.M. Stefanescu, D.K. Bandyopadhyay, On the solidification kinetics of spheroidal graphite cast iron, in: Proceedings of the 3rd International Symposium "Metallurgy of Cast Iron", Tokyo, Japan, 1989, 15-26.
[27] D.K. Banerjee, D.M. Stefanescu, Structural transitions and solidification kinetics of SG cast iron during directional solidification experiments. AFS Transactions 99 (1991) 747-759.
[28] G.L. Rivera, R. Boeri, J. Sikora, Revealing the solidification structure of nodular iron, Cast Metals 8 (1995) 1-5.
[29] D.J. Celentano, P.M. Dardati, L.A. Godoy, R.E. Boeri, Computational simulation of microstructure evolution during solidification of ductile cast iron, International Journal of Cast Metals Research 21 (2008) 416-426.
[30] W. Kapturkiewicz, A.A. Burbelko, M. Górny, Kinetic model of ductile iron solidification with experimental verification, Archives of Foundry Engineering 9 (2009) 95-102.
[31] A.N. Kolmogorov, K statističeskoj teorii kristallizacii metallov, Izvestiya Akademii Nauk SSSR 3 (1937) 355-359 (in Russian).
[32] W. Oldfield, A quantitative approach to casting solidification. Freezing of cast iron, Transactions ASM 59 (1966) 945-961.
[33] E. Fraś, K. Wiencek, M. Górny, H. Lopez, Nucleation and grains density - a theoretical model and experimental verification, Archives of Metallurgy 46 (2001) 317-333.
[34] R. Döpp, The Metallurgy of Cast Iron, Georgi Publishing
[35] D. M. Stefanescu, Science and Engineering of Casting Solidification second ed., Springer Verlag, 2008.
[36] F. Neumann, The influence of additional elements on the physics chemical behavior of carbon in carbon saturated molten iron, recent research in cast iron, Gordon and Breach, New York, 1968.
[37] E. Fraś, K. Wiencek, M. Górny, H.F. Lopez, Nodule count in ductile iron: theoretical model based on Weibull statistic, International Journal of Cast Metals Research 18 (2005) 156-162.
[38] K. Wiencek, J. Ryś, The estimation of Fe_3C particle density in steel by simple counting measurements made in plan sections, Materials Engineering 3 (1998) 396-399.
[39] B. Chopard, M. Droz, Cellular automata modeling of physical systems, Cambridge University Press, Cambridge, UK, 2005.
[40] J. Hoyt, M. Asta, Atomistic computation of liquid diffusivity, solid-liquid interfacial free energy, and kinetic coefficient in Au and Ag, PhysICS Review B 65/214106 (2002) 1–11.
[41] A. Burbelko, Mezomodeling of solidificatnion using a cellular automaton, UWND AGH, 2004, Crakow (in Polish).
[42] W.W. Mullins, R.F. Sekerka, Morphological stability of a particle growing by diffusion or heat flow, Journal of Applied Physics 34 (1963) 323-329.
[43] U. Dilthley, V. Pavlik, Numerical simulation of dendrite morphology and grain growth with modified cellular automata, Modeling of Casting, Welding and Advanced Solidification Processes VIII, TMS, Warrendale, 1998, 589-596.
[44] A.A. Burbelko, W. Kapturkiewicz, D. Gurgul, Analysis of causes and means to reduce artificial anisotropy in modelling of the solidification process on cellular automaton, Solidification Processing 2007, Proceedings of the 5th Decennial International Conference on Solidification Processing, The University of Sheffield, UK, 2007, 31-35.
[45] O.Kubaschewski, Iron – Binary Phase Diagrams, Springer-Verlag, Berlin, 1985.
[46] Ch.A. Gandin, M. Rappaz, A coupled finite element-cellular automaton model for the prediction of dendritic grain structures in solidification processes, Acta Metallurgica et Materialia 42 (1994) 2233-2246.
[47] G. Rivera, R. Boeri, J. Sikora, Revealing and characterising solidification structure of ductile cast iron, Materials Science and Technology 18 (2002) 691-697.
[48] G. Rivera, P.R. Calvillo, R. Boeri, Y. Houbaert, J. Sikora, Examination of the solidification macrostructure of spheroidal and flake graphite cast irons using DAAS and ESBD, Materials Characterization 59 (2008) 1342-1348.